Electronic Supplementary Material (ESI) for ChemComm.

# Supporting Information

# Bulk ionic screening lengths from extremely large-scale molecular dynamics simulations

Johannes Zeman[1], Svyatoslav Kondrat[2,3,4], and Christian Holm*[1]

[1]Institute for Computational Physics, University of Stuttgart, D-70569 Stuttgart, Germany
[2]Department of Complex Systems, Institute of Physical Chemistry, Polish Academy of Sciences,
Kasprzaka 44/52, 01-224 Warsaw, Poland
[3]Max-Planck-Institut für Intelligente Systeme, Heisenbergstraße 3, 70569 Stuttgart, Germany
[4]IV. Institut für Theoretische Physik, Universität Stuttgart, Pfaffenwaldring 57, 70569 Stuttgart, Germany

---

*E-mail: holm@icp.uni-stuttgart.de

# S1 Simulated Systems

Table S1 below lists the compositions of all investigated systems, and ball-and-stick models with the corresponding Lewis formulas are shown in fig. S1.

| $c\,(\mathrm{mol/l})$ | $N_{\mathrm{IP}}$ | $N_{\mathrm{S}}$ | $\bar{L}\,(\mathrm{nm})$ | $t_{\mathrm{sim}}\,(\mathrm{ns})$ | $t_{\mathrm{eq}}\,(\mathrm{ns})$ |
|---|---|---|---|---|---|
| pure $[C_4C_1Im]^+$ $[PF_6]^-$ (all-atom) | | | | | |
| 4.63 | 108,000 | 0 | 33.84 | 600 | 300 |
| pure $[C_4C_1Im]^+$ $[PF_6]^-$ (coarse-grained) | | | | | |
| 4.78 | 358,296 | 0 | 49.92 | 700 | 300 |
| NaCl in water (all-atom) | | | | | |
| 4.43 | 216,000 | 2,458,296 | 43.25 | 200 | 50 |
| 1.16 | 3,750 | 176,577 | 17.53 | 537 | 50 |
| 2.43 | 3,750 | 81,814 | 13.68 | 5369 | 50 |
| 4.86 | 3,750 | 38,411 | 10.86 | 5369 | 50 |
| 5.19 | 3,750 | 35,625 | 10.63 | 5369 | 50 |
| $[C_4C_1Im]^+$ $[NTf_2]^-$ in PC (all-atom) | | | | | |
| 0.00 | 0 | 1,000 | 5.19 | 1074 | 100 |
| 0.53 | 200 | 3,800 | 8.54 | 2147 | 200 |
| 0.97 | 500 | 4,500 | 9.51 | 2147 | 200 |
| 1.63 | 500 | 2,000 | 7.99 | 3221 | 200 |
| 2.10 | 500 | 1,167 | 7.34 | 4295 | 200 |
| 2.47 | 500 | 750 | 6.96 | 4295 | 200 |
| 2.75 | 500 | 500 | 6.71 | 4295 | 200 |
| 2.98 | 500 | 333 | 6.53 | 4295 | 200 |
| 3.17 | 500 | 214 | 6.40 | 4295 | 200 |
| 3.33 | 500 | 125 | 6.30 | 4295 | 200 |
| 3.46 | 500 | 56 | 6.21 | 4295 | 200 |
| 3.58 | 500 | 0 | 6.15 | 4295 | 200 |

**Table S1:** System compositions. Listed values are: molar ion pair concentration $c\,(\mathrm{mol/l})$, number of ion pairs $N_{\mathrm{IP}}$, the number of solvent molecules $N_{\mathrm{S}}$, average simulation box edge length $\bar{L}\,(\mathrm{nm})$, total simulation time $t_{\mathrm{sim}}\,(\mathrm{ns})$ after equilibration, and equilibration time $t_{\mathrm{eq}}\,(\mathrm{ns})$. Further details with corresponding error estimates can be found in section S2.1.

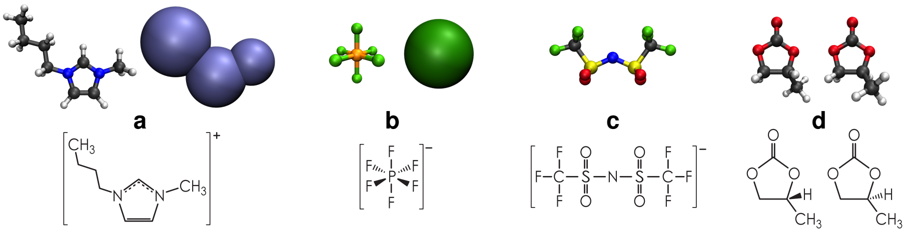

**Figure S1:** Ball-and-stick models (top row, produced with VMD[S1]) and corresponding Lewis formulas (bottom row) of the investigated substances. **a**: 1-butyl-3-methylimidazolium ($[C_4C_1Im]^+$) cation (all-atom (left) and coarse-grained (right)). **b**: hexafluorophosphate ($[PF_6]^-$) anion (all-atom (left) coarse-grained (right)). **c**: bis(trifluoromethylsulfonyl)imide ($[NTf_2]^-$) anion. **d**: (R)-propylene carbonate (left) and (S)-propylene carbonate (right).

# S2 Additional Results

## S2.1 Volumetric system properties

pure $[\mathrm{C_4C_1Im}]^+\,[\mathrm{PF_6}]^-$ (all-atom)

| $c\,(\mathrm{mol/l})$ | $\bar{V}\,(\mathrm{nm}^3)$ | $\bar{\varrho}\,(\mathrm{kg/m}^3)$ | $\varrho_{\mathrm{exp}}\,(\mathrm{kg/m}^3)$ | $\Delta\varrho\,(\%)$ |
|---:|---:|---:|---:|---:|
| 4.62987(4) | 38,735.0(3) | 1,315.735(10) | 1,360.47 | -3.29 |

pure $[\mathrm{C_4C_1Im}]^+\,[\mathrm{PF_6}]^-$ (coarse-grained)

| $c\,(\mathrm{mol/l})$ | $\bar{V}\,(\mathrm{nm}^3)$ | $\bar{\varrho}\,(\mathrm{kg/m}^3)$ | $\varrho_{\mathrm{exp}}\,(\mathrm{kg/m}^3)$ | $\Delta\varrho\,(\%)$ |
|---:|---:|---:|---:|---:|
| 4.78280(2) | 124,396.7(5) | 1,359.223(6) | 1,360.47 | -0.09 |

$[\mathrm{C_4C_1Im}]^+\,[\mathrm{NTf_2}]^-$ in PC (all-atom)

| $c\,(\mathrm{mol/l})$ | $\bar{V}\,(\mathrm{nm}^3)$ | $\bar{\varrho}\,(\mathrm{kg/m}^3)$ | $\varrho_{\mathrm{exp}}\,(\mathrm{kg/m}^3)$ | $\Delta\varrho\,(\%)$ |
|---:|---:|---:|---:|---:|
| 0.00000(0) | 139.46(5) | 1,215.5(4) | 1,197.30 | 1.52 |
| 0.53340(1) | 622.628(5) | 1,258.31(1) | 1,229.92 | 2.31 |
| 0.96600(1) | 859.490(1) | 1,292.67(1) | 1,262.49 | 2.39 |
| 1.62504(1) | 510.922(1) | 1,345.08(1) | 1,307.08 | 2.91 |
| 2.10316(1) | 394.772(3) | 1,383.12(1) | 1,339.01 | 3.29 |
| 2.46649(2) | 336.619(3) | 1,412.06(1) | 1,363.58 | 3.56 |
| 2.75140(2) | 301.763(3) | 1,434.72(1) | 1,382.19 | 3.80 |
| 2.98136(3) | 278.487(3) | 1,452.98(2) | 1,396.75 | 4.03 |
| 3.17022(4) | 261.896(3) | 1,467.99(2) | 1,408.63 | 4.21 |
| 3.32780(4) | 249.495(3) | 1,480.49(2) | 1,418.32 | 4.38 |
| 3.46103(7) | 239.891(5) | 1,491.00(3) | 1,426.15 | 4.55 |
| 3.57732(5) | 232.092(3) | 1,500.20(2) | 1,432.52 | 4.72 |

NaCl in SPC/E water (all-atom)

| $c\,(\mathrm{mol/l})$ | $\bar{V}\,(\mathrm{nm}^3)$ | $\bar{\varrho}\,(\mathrm{kg/m}^3)$ | $\varrho_{\mathrm{exp}}\,(\mathrm{kg/m}^3)$ | $\Delta\varrho\,(\%)$ |
|---:|---:|---:|---:|---:|
| 1.155534(2) | 5,388.87(1) | 1,047.766(2) | 1,042.34 | 0.52 |
| 2.432431(8) | 2,559.999(8) | 1,098.209(4) | 1,090.56 | 0.70 |
| 4.433304(9) | 80,905.0(2) | 1,168.069(2) | 1,162.79 | 0.45 |
| 4.86353(2) | 1,280.349(5) | 1,181.711(5) | 1,178.07 | 0.31 |
| 5.19117(3) | 1,199.541(7) | 1,191.838(7) | 1,189.70 | 0.18 |

**Table S2:** Volumetric system properties. The listed values are molar ion pair concentration $c\,(\mathrm{mol/l})$, average simulation box volume $\bar{V}\,(\mathrm{nm}^3)$, average mass density $\bar{\varrho}\,(\mathrm{kg/m}^3)$, experimental mass density $\varrho_{\mathrm{exp}}\,(\mathrm{kg/m}^3)$, and relative deviation $\Delta\varrho = \frac{\bar{\varrho}-\varrho_{\mathrm{exp}}}{\varrho_{\mathrm{exp}}}$ (%). The experimental value of $\varrho_{\mathrm{exp}}$ for $[\mathrm{C_4C_1Im}]^+\,[\mathrm{PF_6}]^-$ at 300 K is a linear extrapolation of temperature-dependent mass density measurements taken from Machida *et al.*,[S2] whereas the values of $\varrho_{\mathrm{exp}}$ for $[\mathrm{C_4C_1Im}]^+\,[\mathrm{NTf_2}]^-$ in PC are linear interpolations of temperature- and concentration-dependent measurements obtained from Vraneš *et al.*[S3] For aqueous NaCl, the values of $\varrho_{\mathrm{exp}}$ are linear inter- and extrapolations of temperature- and concentration-dependent data from ref. S4.

## S2.2 Static relative dielectric permittivities

$[C_4C_1Im]^+ [NTf_2]^-$ in PC

| $x$ | $c$ (mol/l) | $\varepsilon_r$ | $\lambda_D$ (nm) | $\lambda_S$ (nm) |
|---|---|---|---|---|
| 0.00 | 0.00 | 59.3(6) | — | — |
| 0.05 | 0.53 | 46(3) | 0.32(1) | 0.67(3) |
| 0.10 | 0.97 | 39(5) | 0.22(1) | 0.65(4) |
| 0.20 | 1.63 | 28(3) | 0.144(8) | 0.496(8) |
| 0.30 | 2.10 | 23(3) | 0.114(8) | 0.465(6) |
| 0.40 | 2.47 | 20(3) | 0.099(7) | 0.584(9) |
| 0.50 | 2.75 | 15(2) | 0.081(6) | 0.607(4) |
| 0.60 | 2.98 | 13(2) | 0.073(4) | 0.686(4) |
| 0.70 | 3.17 | 12(1) | 0.068(3) | 0.753(6) |
| 0.80 | 3.33 | 10.0(8) | 0.060(2) | 0.846(8) |
| 0.90 | 3.46 | 10.5(7) | 0.060(2) | 0.95(1) |
| 1.00 | 3.58 | 9.1(5) | 0.055(1) | 1.07(1) |

aqueous NaCl

| $x$ | $c$ (mol/l) | $\varepsilon_r$ | $\lambda_D$ (nm) | $\lambda_S$ (nm) |
|---|---|---|---|---|
| 0.02 | 1.16 | 53(2) | 0.233(3) | 0.25(1) |
| 0.04 | 2.43 | 47(4) | 0.151(6) | 0.197(8) |
| 0.09 | 4.86 | 35(3) | 0.093(4) | 0.32(2) |
| 0.10 | 5.19 | 33(3) | 0.087(4) | 0.33(1) |

**Table S3:** Static relative permittivities $\varepsilon_r$, Debye lengths $\lambda_D$, and effective screening lengths $\lambda_S$ for solutions of $[C_4C_1Im]^+ [NTf_2]^-$ in PC (top) and NaCl in water (bottom) at different concentrations. The numbers in parentheses represent the uncertainty of the last digit.

## S2.3 PMF behavior over time

As stated in the main article, when analyzing simulations of concentrated ionic liquid systems, it is crucial that enough simulation time has been allowed for such systems to reach thermal equilibrium. The following plots show how the PMFs of the largest investigated systems (pure $[\mathrm{C_4C_1Im}]^+\,[\mathrm{PF_6}]^-$, AA and CG models) change over time.

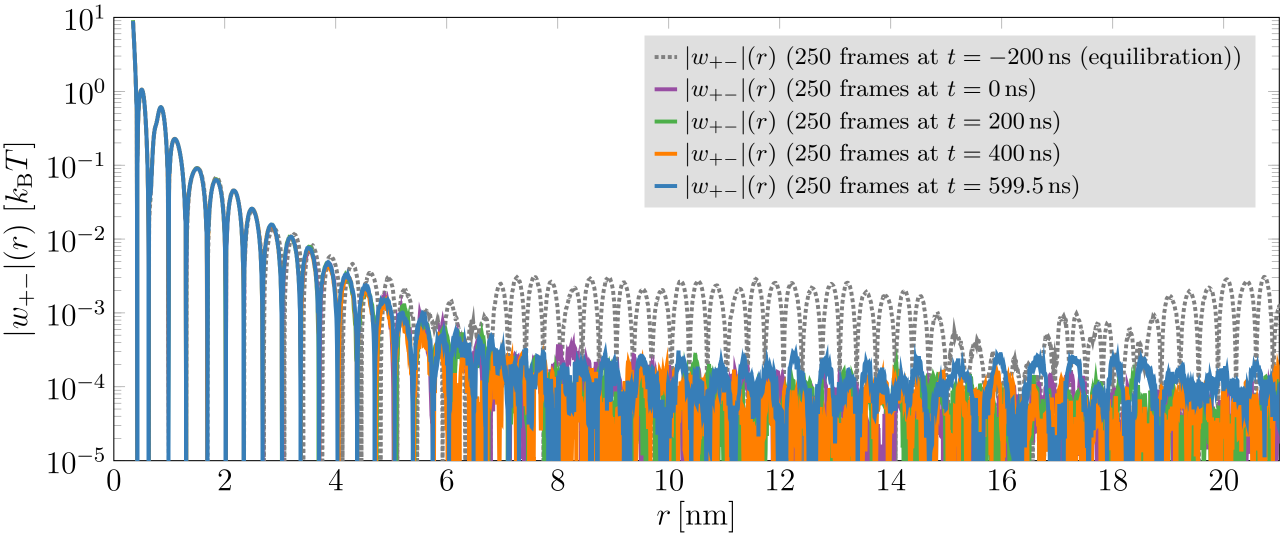

**Figure S2:** Absolute value of the potential of mean force $|w_{+-}|(r)$ between anions and cations in neat $[\mathrm{C_4C_1Im}]^+\,[\mathrm{PF_6}]^-$ (AA model) for 250 analyzed frames (corresponding to a time span $\Delta t = 0.5$ ns) taken at different time steps $t$ during the simulation. The first PMF at $t = -200$ ns (dashed gray line) was computed from trajectory data during system equilibration. Even though its short-range behavior is similar to the remaining PMF curves, this PMF exhibits comparatively large-amplitude, regular oscillations in its tail, showing that the system is not properly equilibrated at this point in time. The remaining PMFs were computed for the same number of frames but at times $t \in \{0, 200, 400, 599.5\}$ ns after equilibration. After equilibration, all PMFs show the same qualitative behavior with rather noisy tails of similar amplitude, demonstrating that the system has reached an equilibrium state.

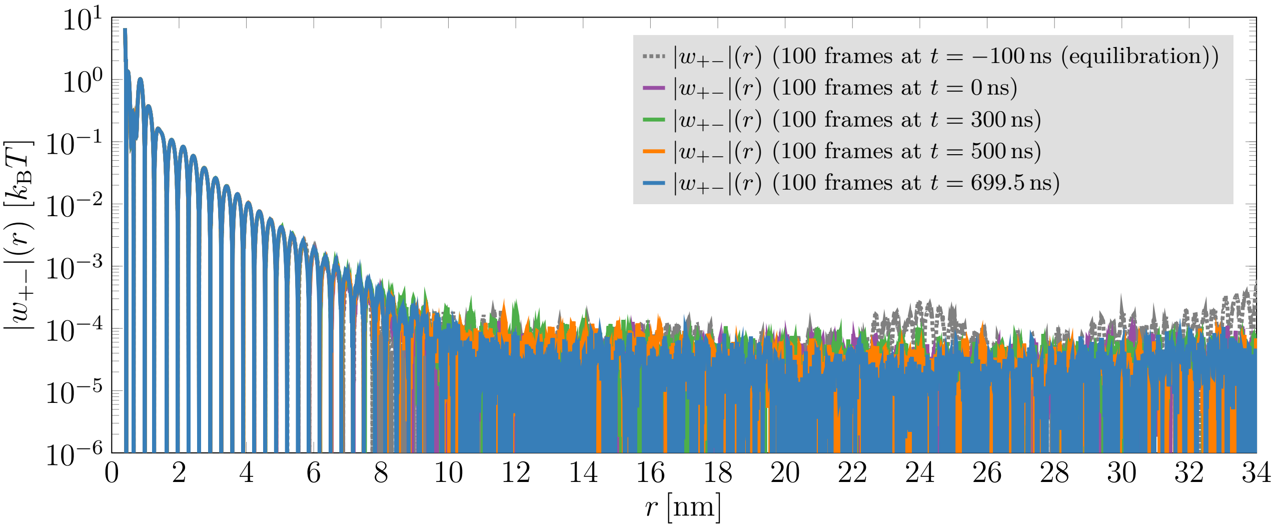

**Figure S3:** Absolute value of the potential of mean force $|w_{+-}|(r)$ between anions and cations in neat $[\mathrm{C_4C_1Im}]^+\,[\mathrm{PF_6}]^-$ (CG model) for 100 analyzed frames (corresponding to a time span $\Delta t = 0.5$ ns) taken at different time steps $t$ during the simulation. The first PMF at $t = -100$ ns (dashed gray line) was computed from trajectory data during system equilibration. It is clearly visible that there are small structural artifacts in the PMF tail at $r \approx 24$ nm and for $r > 29$ nm, showing that the system is not yet equilibrated at this point in time. The remaining PMFs were computed for the same number of frames but at times $t \in \{0, 300, 500, 699.5\}$ ns after equilibration. Obviously, the structural artifacts have vanished after equilibration, and all PMFs show the same qualitative behavior, demonstrating that the system is indeed equilibrated.

The PMFs shown in the above figs. S2 and S3 demonstrate that the systems are properly equilibrated, however, they do not yield implications about the relaxation of the *cumulative* PMF behavior over time. Therefore, the following figs. S4 and S5 show the PMFs' relaxation behavior depending on the number of analyzed frames after equilibration.

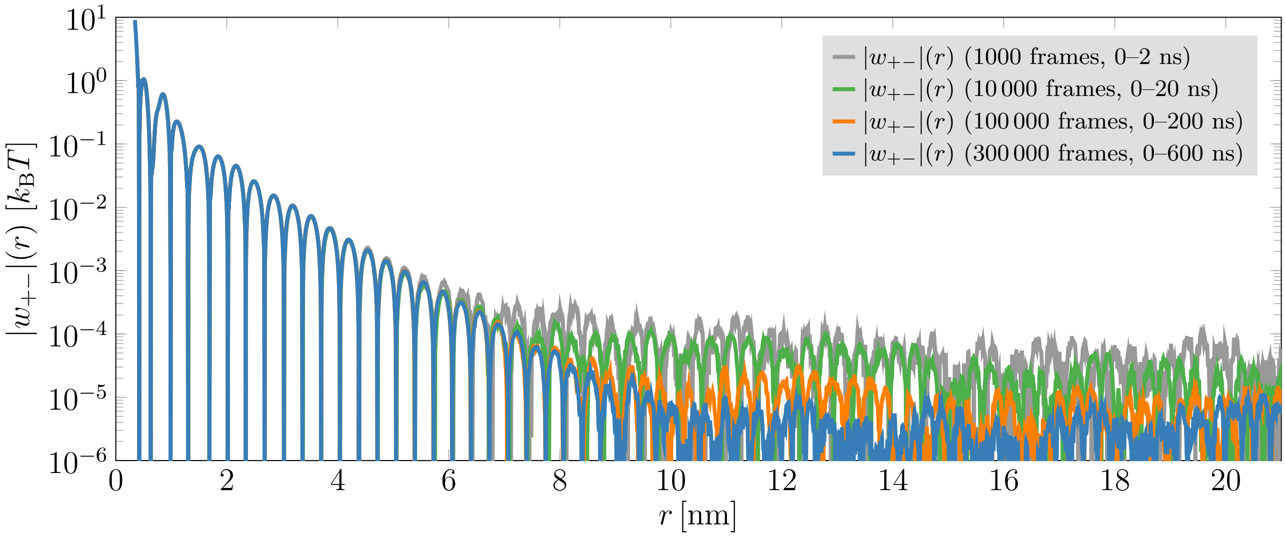

**Figure S4:** Absolute value of the potential of mean force $|w_{+-}|(r)$ between anions and cations in neat $[\mathrm{C_4C_1Im}]^+$ $[\mathrm{PF_6}]^-$ (AA model) for different numbers of analyzed frames (i.e., time spans). Regardless of the number of analyzed frames, the PMFs exhibit an exponentially damped oscillatory behavior, followed by rather noisy oscillations of almost constant amplitude. As the number of analyzed frames increases, the extent of the exponentially damped region increases to larger distances and the amplitude of the oscillatory tail decreases. However, there is no sign of any long-range monotonic decay.

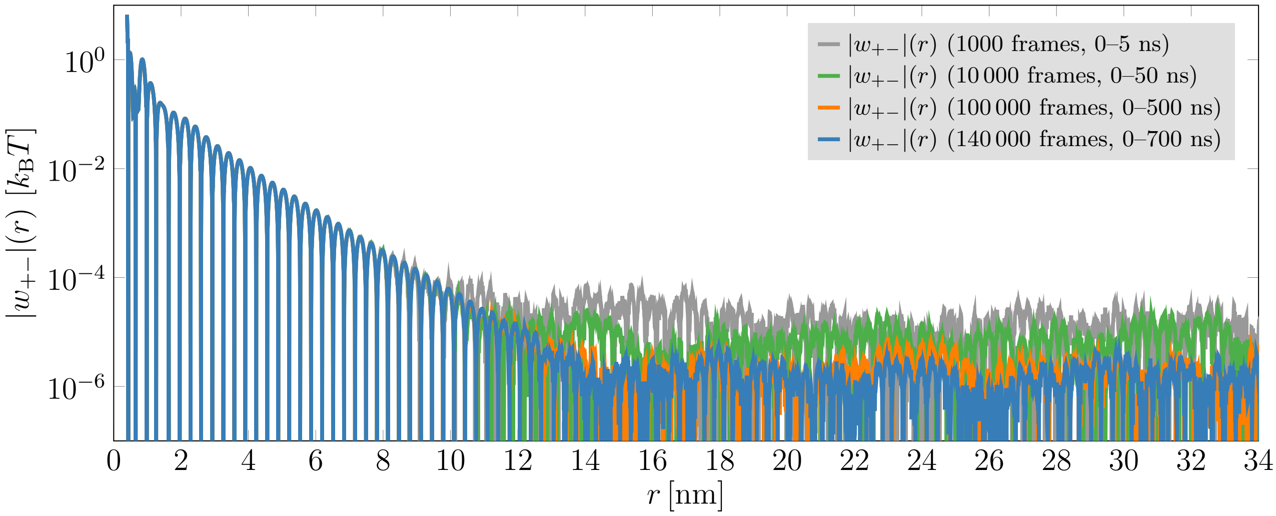

**Figure S5:** Absolute value of the potential of mean force $|w_{+-}|(r)$ between anions and cations in neat $[\mathrm{C_4C_1Im}]^+$ $[\mathrm{PF_6}]^-$ (CG model) for different numbers of analyzed frames (i.e., time spans). As for the all-atom model, the PMFs exhibit an exponentially damped oscillatory behavior, followed by rather noisy oscillations of almost constant amplitude. Likewise, as the number of analyzed frames increases, the extent of the exponentially damped region increases to larger distances and the amplitude of the oscillatory tail decreases. Again, there is no sign of any long-range monotonic decay.

For both molecular models, the extent of the damped oscillatory region increases with simulation time but the qualitative PMF behavior remains unchanged and without any indication for a long-ranged, monotonic decay.

## S2.4 Screening length scaling analysis of $[C_4C_1Im]^+ [NTf_2]^-$ in propylene carbonate

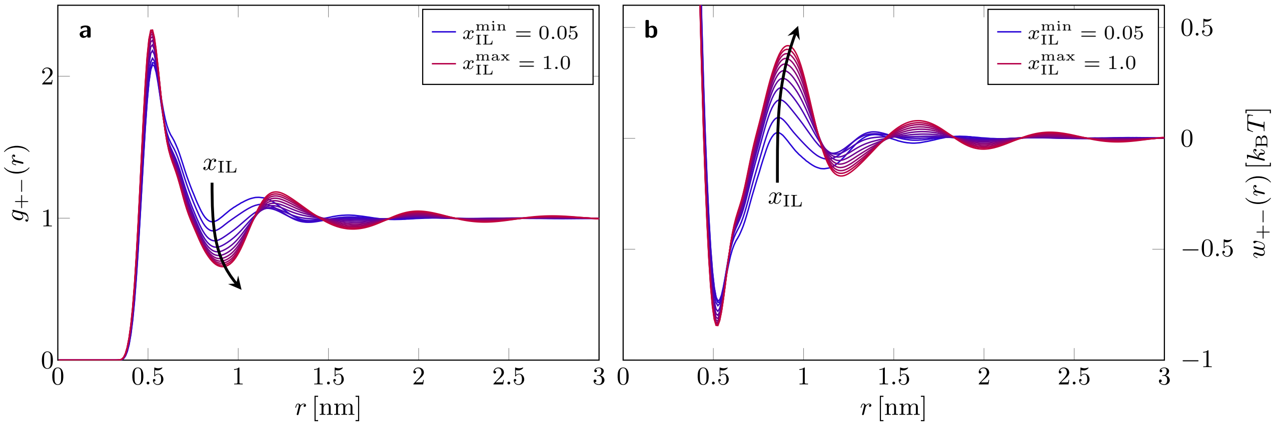

**Figure S6:** Panel **a**: Cation-anion radial distribution functions $g_{+-}(r)$ of $[C_4C_1Im]^+ [NTf_2]^-$ in propylene carbonate for different IL mole fractions $x$ ranging from $x = 0.05$ (blue) to $x = 1.0$ (red). Panel **b**: Corresponding cation-anion potentials of mean force $w_{+-}(r)$ of the same systems (same color code). Arrows indicate increasing IL mole fraction.

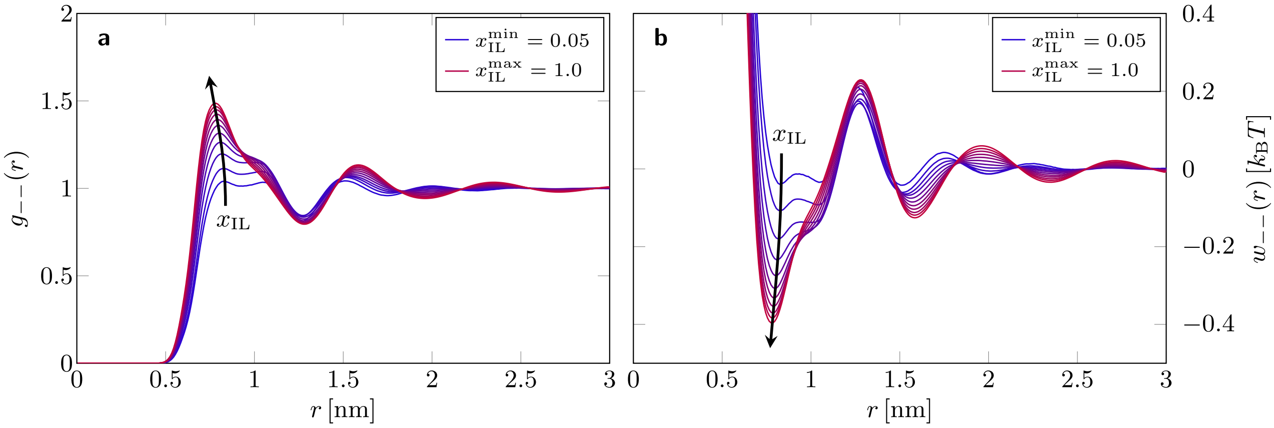

**Figure S7:** Panel **a**: Anion-anion radial distribution functions $g_{--}(r)$ of $[C_4C_1Im]^+ [NTf_2]^-$ in propylene carbonate for different IL mole fractions $x$ ranging from $x = 0.05$ (blue) to $x = 1.0$ (red). Panel **b**: Corresponding anion-anion potentials of mean force $w_{--}(r)$ of the same systems (same color code). Arrows indicate increasing IL mole fraction.

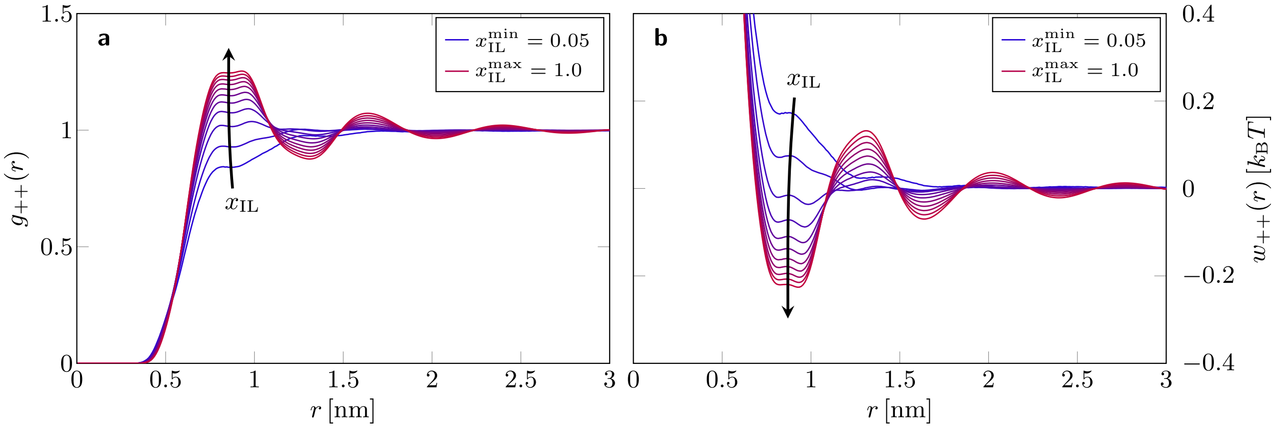

**Figure S8:** Panel **a**: Cation-cation radial distribution functions $g_{++}(r)$ of $[C_4C_1Im]^+ [NTf_2]^-$ in propylene carbonate for different IL mole fractions $x$ ranging from $x = 0.05$ (blue) to $x = 1.0$ (red). Panel **b**: Corresponding cation-cation potentials of mean force $w_{++}(r)$ of the same systems (same color code). Arrows indicate increasing IL mole fraction.

Listed below in tables S4 to S6 are the parameters resulting from fits of a superposition of $k = 2$ oscillatory, exponentially damped hyperbolas of the form

$$f(r) = \sum_{n=1}^{k} \frac{A_n}{r} \cos\left(\omega_n r - \phi_n\right) \exp\left(-\frac{r}{\lambda_n}\right) \tag{S1}$$

to the PMFs in solutions of $[\mathrm{C_4C_1Im}]^+\,[\mathrm{NTf_2}]^-$ in propylene carbonate at different IL mole fractions $x$.

| $x$ | $c_{\mathrm{IL}}$ (mol/l) | $A_1$ ($k_{\mathrm{B}}T$) | $\lambda_1$ (nm) | $2\pi/\omega_1$ (nm) | $\phi_1$ | $A_2$ ($k_{\mathrm{B}}T$) | $\lambda_2$ (nm) | $2\pi/\omega_2$ (nm) | $\phi_2$ | $R^2$ |
|---|---|---|---|---|---|---|---|---|---|---|
| 0.05 | 0.53 | 1.11(4) | 0.444(5) | 0.477(1) | 5.83(5) | -15(2) | 0.222(3) | $\infty$ | — | 0.9955 |
| 0.10 | 0.97 | 1.13(7) | 0.404(6) | 0.458(1) | 0.38(7) | 9534(5496) | 0.158(7) | 116(1) | 2(44) | 0.9948 |
| 0.20 | 1.63 | 0.39(2) | 0.496(8) | 0.465(3) | 5.87(5) | 2.8(2) | 0.309(5) | 0.799(3) | 6.04(6) | 0.9980 |
| 0.30 | 2.10 | 0.79(8) | 0.41(1) | 0.468(6) | 5.6(1) | 1.6(1) | 0.395(7) | 0.729(3) | 1.37(7) | 0.9966 |
| 0.40 | 2.47 | 1.16(9) | 0.373(7) | 0.465(5) | 5.6(1) | 1.42(5) | 0.462(4) | 0.731(1) | 1.56(3) | 0.9990 |
| 0.50 | 2.75 | 1.5(1) | 0.348(6) | 0.461(5) | 5.84(9) | 1.14(2) | 0.555(3) | 0.7383(8) | 1.50(2) | 0.9996 |
| 0.60 | 2.98 | 1.7(1) | 0.339(6) | 0.464(5) | 5.73(9) | 1.02(1) | 0.636(3) | 0.7409(6) | 1.45(1) | 0.9997 |
| 0.70 | 3.17 | 1.5(1) | 0.351(6) | 0.467(5) | 5.55(9) | 0.99(1) | 0.700(3) | 0.7446(5) | 1.35(1) | 0.9998 |
| 0.80 | 3.33 | 1.6(2) | 0.343(8) | 0.468(7) | 5.5(1) | 0.90(1) | 0.786(4) | 0.7457(5) | 1.32(1) | 0.9998 |
| 0.90 | 3.46 | 1.6(2) | 0.34(1) | 0.468(8) | 5.53(1) | 0.83(1) | 0.871(5) | 0.7471(5) | 1.28(1) | 0.9997 |
| 1.00 | 3.58 | 2.0(3) | 0.33(1) | 0.48(1) | 5.1(2) | 0.81(1) | 0.941(7) | 0.7457(5) | 1.28(1) | 0.9997 |

**Table S4:** Fit parameters of eq. (S1) to cation-anion PMFs $w_{+-}(r)$ in solutions of $[\mathrm{C_4C_1Im}]^+\,[\mathrm{NTf_2}]^-$ in propylene carbonate for different mole fractions $x$ in the fit range $1.2 \leqslant r \leqslant 3.0\,\mathrm{nm}$. The values (units) are IL mole fraction $x$, concentration $c$ (mol/l), amplitudes $A_n$ ($k_{\mathrm{B}}T$), wavelengths $2\pi/\omega_n$ (nm), phase shifts $\phi_n$, and the coefficient of determination $R^2$. The numbers in parentheses represent the uncertainty of the last digit.

| $x$ | $c_{\mathrm{IL}}$ (mol/l) | $A_1$ ($k_{\mathrm{B}}T$) | $\lambda_1$ (nm) | $2\pi/\omega_1$ (nm) | $\phi_1$ | $A_2$ ($k_{\mathrm{B}}T$) | $\lambda_2$ (nm) | $2\pi/\omega_2$ (nm) | $\phi_2$ | $R^2$ |
|---|---|---|---|---|---|---|---|---|---|---|
| 0.05 | 0.53 | 3.8(1) | 0.421(4) | 0.4843(7) | 4.09(3) | 4.3(4) | 0.308(7) | $\infty$ | — | 0.9976 |
| 0.10 | 0.97 | 0.9(1) | 0.56(1) | 0.463(2) | 5.4(1) | 88(10) | 0.201(4) | 0.489(4) | 3.7(1) | 0.9995 |
| 0.20 | 1.63 | 3.8(2) | 0.389(5) | 0.475(3) | 4.61(7) | 1.9(2) | 0.36(1) | 0.714(5) | 4.8(1) | 0.9991 |
| 0.30 | 2.10 | 3.5(2) | 0.382(4) | 0.469(3) | 4.94(5) | 1.75(5) | 0.465(6) | 0.720(2) | 4.82(4) | 0.9996 |
| 0.40 | 2.47 | 3.5(1) | 0.373(4) | 0.466(2) | 5.16(5) | 1.69(5) | 0.522(4) | 0.723(1) | 4.79(2) | 0.9998 |
| 0.50 | 2.75 | 3.8(2) | 0.358(4) | 0.466(3) | 5.24(5) | 1.40(3) | 0.607(4) | 0.7282(7) | 4.70(2) | 0.9998 |
| 0.60 | 2.98 | 4.0(2) | 0.349(4) | 0.464(3) | 5.37(5) | 1.23(2) | 0.686(4) | 0.7310(7) | 4.63(1) | 0.9998 |
| 0.70 | 3.17 | 5.0(4) | 0.329(5) | 0.464(4) | 5.46(8) | 1.13(2) | 0.753(6) | 0.7342(7) | 4.54(2) | 0.9997 |
| 0.80 | 3.33 | 6.3(6) | 0.312(6) | 0.468(6) | 5.4(1) | 0.98(2) | 0.846(8) | 0.7371(8) | 4.46(1) | 0.9996 |
| 0.90 | 3.46 | 7.5(9) | 0.303(7) | 0.476(7) | 5.1(1) | 0.85(2) | 0.95(1) | 0.7394(8) | 4.40(2) | 0.9995 |
| 1.00 | 3.58 | 8(1) | 0.296(8) | 0.479(8) | 5.0(1) | 0.76(2) | 1.07(1) | 0.7388(9) | 4.38(2) | 0.9994 |

**Table S5:** Fit parameters of eq. (S1) to anion-anion PMFs $w_{--}(r)$ in solutions of $[\mathrm{C_4C_1Im}]^+\,[\mathrm{NTf_2}]^-$ in propylene carbonate for different mole fractions $x$ in the fit range $1.2 \leqslant r \leqslant 3.0\,\mathrm{nm}$. The values (units) are IL mole fraction $x$, concentration $c$ (mol/l), amplitudes $A_n$ ($k_{\mathrm{B}}T$), wavelengths $2\pi/\omega_n$ (nm), phase shifts $\phi_n$, and the coefficient of determination $R^2$. The numbers in parentheses represent the uncertainty of the last digit.

| $x$ | $c_{\mathrm{IL}}$ (mol/l) | $A_1$ ($k_{\mathrm{B}}T$) | $\lambda_1$ (nm) | $2\pi/\omega_1$ (nm) | $\phi_1$ | $A_2$ ($k_{\mathrm{B}}T$) | $\lambda_2$ (nm) | $2\pi/\omega_2$ (nm) | $\phi_2$ | $R^2$ |
|---|---|---|---|---|---|---|---|---|---|---|
| 0.05 | 0.53 | 0.09(1) | 0.67(3) | 0.47(1) | 0.7(1) | 2.8(2) | 0.302(4) | $\infty$ | — | 0.9853 |
| 0.10 | 0.97 | 0.07(1) | 0.65(4) | 0.46(2) | 1.0(1) | 0.21(6) | 0.43(3) | 1.11(2) | 6.0(2) | 0.8456 |
| 0.20 | 1.63 | 0.24(3) | 0.46(1) | 0.48(1) | 5.5(1) | 0.18(3) | 0.44(2) | 0.96(2) | 0.3(2) | 0.9868 |
| 0.30 | 2.10 | 56(25) | 0.19(1) | 0.53(2) | 4.3(3) | 0.3(1) | 0.45(3) | 0.86(1) | 1.6(2) | 0.9905 |
| 0.40 | 2.47 | 12(2) | 0.226(6) | 0.50(1) | 5.0(2) | 0.26(2) | 0.58(1) | 0.740(3) | 4.77(7) | 0.9990 |
| 0.50 | 2.75 | 92(34) | 0.169(7) | 0.45(2) | 0.9(4) | 0.50(2) | 0.597(6) | 0.734(2) | 4.95(4) | 0.9991 |
| 0.60 | 2.98 | 12(2) | 0.227(6) | 0.48(1) | 5.3(3) | 0.56(1) | 0.668(3) | 0.730(1) | 5.12(3) | 0.9997 |
| 0.70 | 3.17 | 24(4) | 0.206(4) | 0.47(1) | 5.8(2) | 0.584(7) | 0.744(3) | 0.7394(5) | 4.89(1) | 0.9999 |
| 0.80 | 3.33 | 40(7) | 0.193(4) | 0.46(1) | 0.1(3) | 0.606(6) | 0.815(3) | 0.7411(4) | 4.82(1) | 0.9999 |
| 0.90 | 3.46 | 84(16) | 0.176(4) | 0.43(2) | 1.3(3) | 0.604(5) | 0.895(3) | 0.7444(4) | 4.72(1) | 0.9999 |
| 1.00 | 3.58 | 104(22) | 0.174(4) | 0.43(2) | 1.6(3) | 0.594(4) | 0.983(3) | 0.7432(4) | 4.71(1) | 0.9999 |

**Table S6:** Fit parameters of eq. (S1) to cation-cation PMFs $w_{++}(r)$ in solutions of $[\mathrm{C_4C_1Im}]^+\,[\mathrm{NTf_2}]^-$ in propylene carbonate for different mole fractions $x$ in the fit range $1.2 \leqslant r \leqslant 3.0\,\mathrm{nm}$. The values (units) are IL mole fraction $x$, concentration $c$ (mol/l), amplitudes $A_n$ ($k_{\mathrm{B}}T$), wavelengths $2\pi/\omega_n$ (nm), phase shifts $\phi_n$, and the coefficient of determination $R^2$. The numbers in parentheses represent the uncertainty of the last digit.

Fitting the data to eq. (S1) with $k = 3$ terms resulted in extremely unstable results under slight variation of initial fit parameters, while setting $k = 1$ lead to large fitting errors.

## S2.5 Screening length scaling analysis of NaCl in water

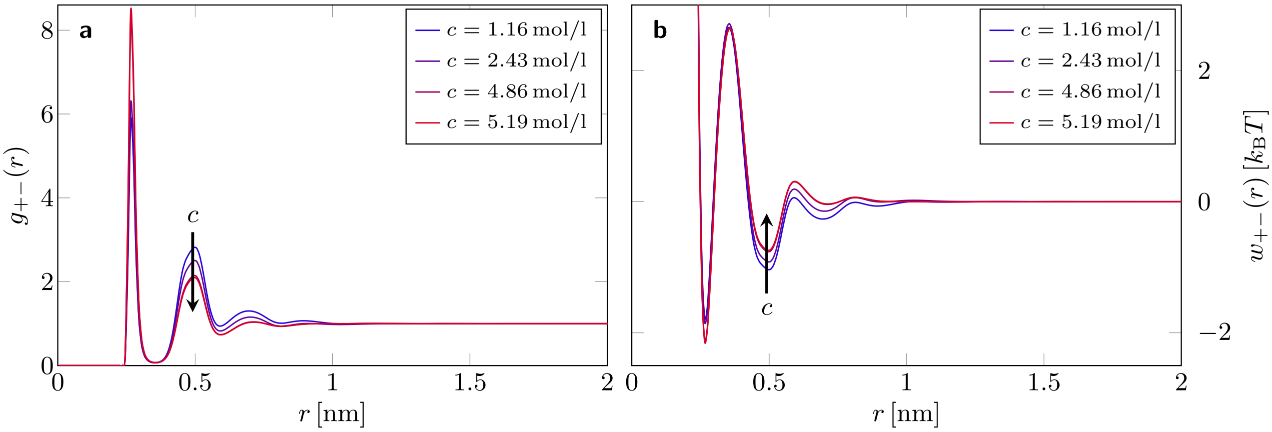

**Figure S9:** Panel **a**: Cation-anion RDFs $g_{+-}(r)$ of aqueous NaCl solutions for different concentrations $c \in \{1.16,\ 2.43,\ 4.86,\ 5.19\}$ mol/l. Panel **b**: Corresponding cation-anion potentials of mean force $w_{+-}(r)$ of the same systems (same color code). Arrows indicate increasing NaCl concentration.

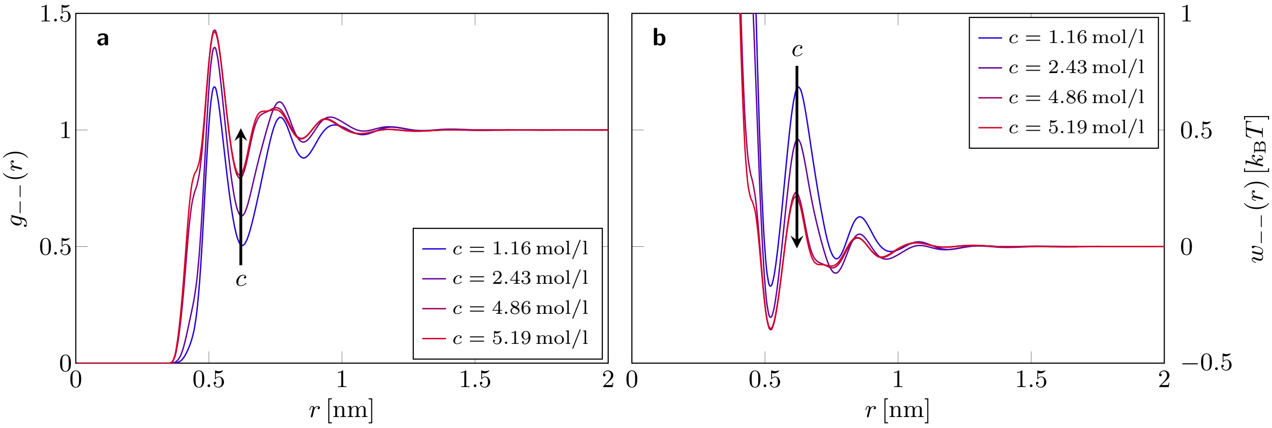

**Figure S10:** Panel **a**: Anion-anion RDFs $g_{--}(r)$ of aqueous NaCl solutions for different concentrations $c \in \{1.16,\ 2.43,\ 4.86,\ 5.19\}$ mol/l. Panel **b**: Corresponding cation-anion potentials of mean force $w_{--}(r)$ of the same systems (same color code). Arrows indicate increasing NaCl concentration.

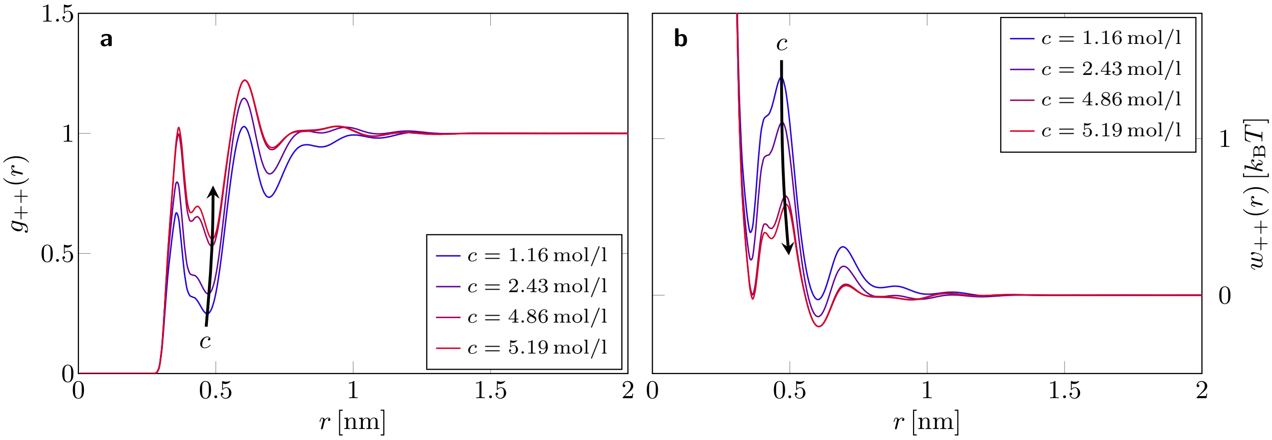

**Figure S11:** Panel **a**: Cation-cation RDFs $g_{++}(r)$ of aqueous NaCl solutions for different concentrations $c \in \{1.16,\ 2.43,\ 4.86,\ 5.19\}$ mol/l. Panel **b**: Corresponding cation-cation potentials of mean force $w_{++}(r)$ of the same systems (same color code). Arrows indicate increasing NaCl concentration.

Listed below in table S7 are the parameters resulting from fits of a superposition of $k = 3$ oscillatory, exponentially damped hyperbolas of the form

$$f(r) = \sum_{n=1}^{k} \frac{A_n}{r} \cos\left(\omega_n r - \phi_n\right) \exp\left(-\frac{r}{\lambda_n}\right) \tag{S2}$$

to the PMFs $w_{+-}(r)$ in aqueous NaCl solutions at different concentrations.

| $c$ (mol/l) | $A_1$ ($k_\mathrm{B}T$) | $\lambda_1$ (nm) | $2\pi/\omega_1$ (nm) | $\phi_1$ | $A_2$ ($k_\mathrm{B}T$) | $\lambda_2$ (nm) | $2\pi/\omega_2$ (nm) | $\phi_2$ |
|---|---|---|---|---|---|---|---|---|
| 1.16 | 3.9(3) | 0.200(2) | 2.372(3) | 4.8(3) | 30(4) | 0.126(2) | 0.209(3) | 5.6(2) |
| 2.43 | 4.2(5) | 0.185(4) | 1.096(1) | 0.0(1) | 1.1(3) | 0.197(8) | 0.289(3) | 3.9(3) |
| 4.86 | 1.4(1) | 0.202(3) | 0.9379(7) | 5.5(1) | 0.09(2) | 0.32(2) | 0.222(1) | 5.7(2) |
| 5.19 | 3.5(3) | 0.170(2) | 0.990(1) | 4.9(1) | 0.08(1) | 0.33(1) | 0.225(1) | 5.0(2) |

| $c$ (mol/l) | $A_3$ ($k_\mathrm{B}T$) | $\lambda_3$ (nm) | $2\pi/\omega_3$ (nm) | $\phi_3$ | $R^2$ |
|---|---|---|---|---|---|
| 1.16 | 0.3(1) | 0.25(1) | 0.303(3) | 3.0(2) | 0.9986 |
| 2.43 | 32408(11376) | 0.062(2) | 0.226(9) | 4.4(5) | 0.9988 |
| 4.86 | 3203(1159) | 0.071(2) | 0.188(3) | 2.4(3) | 0.9990 |
| 5.19 | 634(239) | 0.079(3) | 0.170(4) | 5.4(4) | 0.9986 |

**Table S7:** Fit parameters of eq. (S2) to cation-anion PMFs $w_{+-}(r)$ in solutions for different NaCl concentrations $c$ in the fit range $0.8 \leqslant r \leqslant 2.0\,\mathrm{nm}$. The values (units) are NaCl ion pair concentration $c$ (mol/l), amplitudes $A_n$ ($k_\mathrm{B}T$), wavelengths $2\pi/\omega_n$ (nm), phase shifts $\phi_n$, and the coefficient of determination $R^2$. The numbers in parentheses represent the uncertainty of the last digit.

The scaling plot of $\frac{\lambda_n}{\lambda_\mathrm{D}}$ vs. $\frac{d}{\lambda_\mathrm{D}}$ is shown in fig. S12 for fits to all concentration-dependent cation-anion PMFs $w_{+-}(r)$.

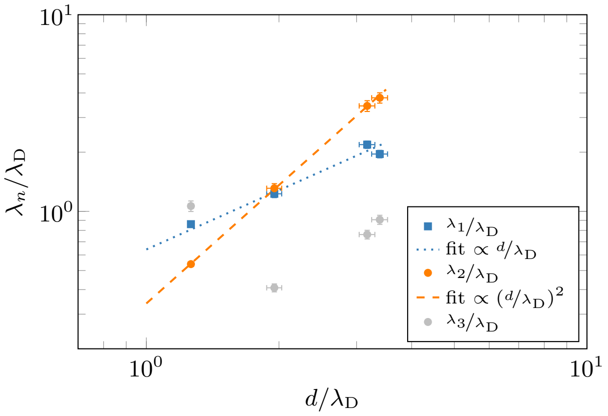

**Figure S12:** Scaling of the fitted screening lengths for all investigated cation-anion PMFs in aqueous NaCl solutions.

While the screening lengths $\lambda_1$ and $\lambda_2$ exhibit a polynomial scaling, the third term with corresponding screening length $\lambda_3$, which was required to obtain a satisfactory fit, does not provide such a clear trend.

Setting $k = 2$ in eq. (S2) lead to much larger fit errors and no clearly identifyable scaling exponents. The corresponding plot is shown in fig. S13 below.

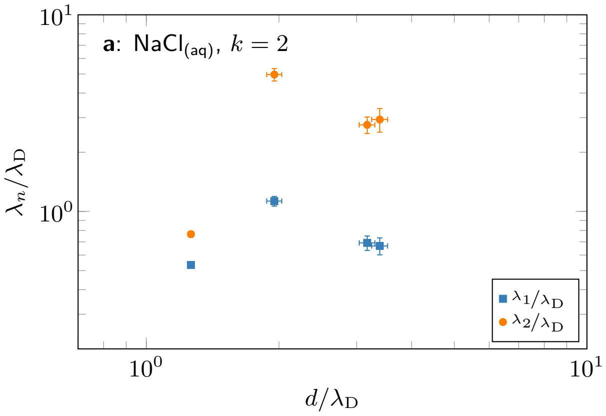

**Figure S13:** Scaling of the fitted screening lengths from eq. (S2) with $k = 2$ terms for all investigated cation-anion PMFs in aqueous NaCl solutions.

# S3 GROMACS Simulation Parameters

All systems were simulated in the $NpT$ ensemble in cubic boxes with periodic boundary conditions in all three dimensions, where temperature and pressure were maintained at $T = 300\,\mathrm{K}$ and $p = 1$ bar using a Nosé-Hoover thermostat and Parrinello-Rahman barostat. Short-range van der Waals interactions were computed up to a system-dependent cut-off, and their long-range part was either computed using the smooth particle mesh Ewald (SPME) method with a relative accuracy of $10^{-3}$, or taken into account via analytic dispersion corrections for energy and pressure. Long-range Coulomb interactions were computed using the SPME method with a short-range cut-off of at least 1.3 nm, a relative accuracy of $10^{-5}$, and tin foil boundary conditions at infinity. The time step of the employed leapfrog integrator was 2 fs for the all-atom models and 5 fs for the coarse-grained IL model.

In the following, we list the GROMACS molecular dynamics parameters used in production runs for all investigated systems.

## S3.1 $[\mathrm{C_4C_1Im}]^+$ $[\mathrm{PF_6}]^-$ (all-atom model)

| **parameter** | **value** | **unit (note)** |
|---|---|---|
| integrator | md | (leapfrog integrator) |
| dt | 0.002 | ps |
| nsteps | 300000000 | steps |
| comm-mode | linear | |
| nstcomm | 50 | steps |
| nstcalcenergy | 50 | steps |
| nstxout-compressed | 1000 | steps |
| compressed-x-precision | 10000 | (means $10^{-4}$ nm) |
| cutoff-scheme | verlet | |
| nstlist | 40 | steps |
| ns-type | grid | |
| pbc | xyz | |
| coulombtype | pme | |
| coulomb-modifier | potential-shift-verlet | |
| rcoulomb | 1.3 | nm |
| vdwtype | pme | |
| vdw-modifier | potential-shift-verlet | |
| rvdw | 1.3 | nm |
| tcoupl | nose-hoover | |
| nsttcouple | 5 | steps |
| nh-chain-length | 1 | |
| tau-t | 2.0 | ps |
| ref-t | 300.0 | K |
| pcoupl | parrinello-rahman | |
| pcoupltype | isotropic | |
| nstpcouple | 5 | steps |
| tau-p | 3.0 | ps |
| compressibility | 4.5e-5 | $\mathrm{bar}^{-1}$ |
| ref-p | 1.0 | bar |
| constraints | h-bonds | (fix length of bonds involving H atoms) |
| constraint-algorithm | lincs | |

**Table S8:** GROMACS molecular dynamics simulation parameters used for the simulation of $[\mathrm{C_4C_1Im}]^+$ $[\mathrm{PF_6}]^-$ (all-atom model). Only parameters which differ from the default (or have no default) are listed.

## S3.2 $[C_4C_1Im]^+ [PF_6]^-$ (coarse-grained model)

| **parameter** | **value** | **unit (note)** |
|---|---|---|
| integrator | md | (leapfrog integrator) |
| dt | 0.005 | ps |
| nsteps | 140000000 | steps |
| comm-mode | linear | |
| nstcomm | 200 | steps |
| nstcalcenergy | 200 | steps |
| nstxout-compressed | 1000 | steps |
| compressed-x-precision | 1000 | (means $10^{-3}$ nm) |
| cutoff-scheme | verlet | |
| nstlist | 40 | steps |
| ns-type | grid | |
| pbc | xyz | |
| coulombtype | pme | |
| coulomb-modifier | potential-shift-verlet | |
| rcoulomb | 1.6 | nm |
| vdwtype | cut-off | |
| vdw-modifier | potential-shift-verlet | |
| dispcorr | enerpres | |
| rvdw | 1.6 | nm |
| tcoupl | nose-hoover | |
| nh-chain-length | 1 | |
| tau-t | 5.0 | ps |
| ref-t | 300.0 | K |
| pcoupl | parrinello-rahman | |
| pcoupltype | isotropic | |
| tau-p | 10.0 | ps |
| compressibility | 4.5e-5 | $\text{bar}^{-1}$ |
| ref-p | 1.0 | bar |
| constraints | all-bonds | (rigid molecular geometry) |
| constraint-algorithm | lincs | |

**Table S9:** GROMACS molecular dynamics simulation parameters used for the simulation of $[C_4C_1Im]^+ [PF_6]^-$ (coarse-grained model). Only parameters which differ from the default (or have no default) are listed.

## S3.3 Aqueous NaCl solutions

| **parameter** | **value** | **unit (note)** |
|---|---|---|
| integrator | md | (leapfrog integrator) |
| dt | 0.002 | ps |
| nsteps | 100000000 | steps |
| comm-mode | linear | |
| nstcomm | 50 | steps |
| nstcalcenergy | 50 | steps |
| nstxout-compressed | 1000 | steps |
| compressed-x-precision | 10000 | (means $10^{-4}$ nm) |
| cutoff-scheme | verlet | |
| nstlist | 40 | steps |
| ns-type | grid | |
| pbc | xyz | |
| coulombtype | p3m-ad | |
| coulomb-modifier | potential-shift-verlet | |
| rcoulomb | 1.2 | nm |
| vdwtype | cut-off | |
| vdw-modifier | potential-shift-verlet | |
| dispcorr | enerpres | |
| rvdw | 1.2 | nm |
| ewald-rtol | 1.0e-6 | |
| tcoupl | nose-hoover | |
| nsttcouple | 5 | steps |
| nh-chain-length | 1 | |
| tau-t | 2.0 | ps |
| ref-t | 300.0 | K |
| pcoupl | parrinello-rahman | |
| pcoupltype | isotropic | |
| nstpcouple | 5 | steps |
| tau-p | 3.0 | ps |
| compressibility | 4.5e-5 | $\text{bar}^{-1}$ |
| ref-p | 1.0 | bar |
| constraints | all-bonds | (rigid water geometry) |
| constraint-algorithm | lincs | |

**Table S10:** GROMACS molecular dynamics simulation parameters used for the simulation of aqueous NaCl solutions. Only parameters which differ from the default (or have no default) are listed.

## S3.4 $[C_4C_1Im]^+ [NTf_2]^-$ in PC

| **parameter** | **value** | **unit (note)** |
|---|---|---|
| integrator | md | (leapfrog integrator) |
| dt | 0.002 | ps |
| nsteps | 1073741824 | steps (= $2^{30}$) |
| comm-mode | linear | |
| nstcomm | 1 | steps |
| nstcalcenergy | 50 | steps |
| nstxout-compressed | 1000 | steps |
| compressed-x-precision | 10000 | (means $10^{-4}$ nm) |
| cutoff-scheme | verlet | |
| nstlist | 40 | steps |
| ns-type | grid | |
| pbc | xyz | |
| coulombtype | pme | |
| coulomb-modifier | potential-shift-verlet | |
| rcoulomb | 1.3 | nm |
| vdwtype | cut-off | |
| vdw-modifier | potential-shift-verlet | |
| dispcorr | enerpres | |
| rvdw | 1.3 | nm |
| tcoupl | nose-hoover | |
| nsttcouple | 5 | steps |
| nh-chain-length | 1 | |
| tau-t | 2.0 | ps |
| ref-t | 300.0 | K |
| pcoupl | parrinello-rahman | |
| pcoupltype | isotropic | |
| nstpcouple | 5 | steps |
| tau-p | 3.0 | ps |
| compressibility | 4.5e-5 | $\text{bar}^{-1}$ |
| ref-p | 1.0 | bar |
| constraints | h-bonds | (fix length of bonds involving H atoms) |
| constraint-algorithm | lincs | |

**Table S11:** GROMACS molecular dynamics simulation parameters used for the simulation of $[C_4C_1Im]^+ [NTf_2]^-$ in propylene carbonate. Only parameters which differ from the default (or have no default) are listed.

# References

[S1] Humphrey, W.; Dalke, A.; Schulten, K. VMD: Visual Molecular Dynamics. *Journal of Molecular Graphics* **1996**, *14*, 33–38, DOI: `10.1016/0263-7855(96)00018-5`.

[S2] Machida, H.; Sato, Y.; Smith Jr., R. L. Pressure-volume-temperature (PVT) measurements of ionic liquids ([bmim$^+$][PF$_6^-$], [bmim$^+$][BF4−], [bmim$^+$][OcSO$_4^-$]) and analysis with the Sanchez-Lacombe equation of state. *Fluid Phase Equilibria* **2008**, *264*, 147–155, DOI: `10.1016/j.fluid.2007.11.005`.

[S3] Vraneš, M.; Zec, N.; Tot, A.; Papović, S.; Dožić, S.; Gadžurić, S. Density, electrical conductivity, viscosity and excess properties of 1-butyl-3-methylimidazolium bis(trifluoromethylsulfonyl)imide + propylene carbonate binary mixtures. *The Journal of Chemical Thermodynamics* **2014**, *68*, 98–108, DOI: `10.1016/j.jct.2013.08.034`.

[S4] Rumble, J. R., Ed. *CRC Handbook of Chemistry and Physics*, 100th ed.; CRC Handbook of Chemistry and Physics; CRC Press / Taylor & Francis: Boca Raton, Florida, 2019.